

Controlling the competitive growth of zeolite phases without using an organic structure-directing agent. Synthesis of Al-rich *BEA

Radim Pilar, Jaroslava Moravkova, Galina Sadovska, Stepan Sklenak, Jiri Brabec, Jana Pastvova, Petr Sazama*

*J. Heyrovsky Institute of Physical Chemistry, Academy of Sciences of the Czech Republic,
Dolejskova 2155/3, 182 23 Prague 8, Czech*

**petr.sazama@jh-inst.cas.cz*

Abstract

*The synthesis of zeolites without using an organic structure-directing agent (OSDA) offers great environmental and economic advantages; however, the zeolites being formed are not stabilized by the organic molecules and kinetic control of the synthesis ensuring high yield and purity of the phases is challenging for many zeolites. For OSDA-free synthesis of an Al-rich *BEA zeolite, this study shows that the zeolite is formed as a metastable phase that can undergo recrystallization immediately after completion of its crystallization to form a thermodynamically more stable MOR zeolite according to Ostwald's rule of stages. The OSDA-free zeolite synthesis is a dynamic process in which crystallization and dissolution occur simultaneously. As soon as a thermodynamically more stable MOR zeolite begins to form in the synthesis mixture, its formation causes depletion of the Al and Si from the synthesis mixture, and, because of the desaturation of the synthesis gel, the original *BEA zeolite begins to dissolve rapidly under hydrothermal conditions. The formation of targeted and parasitic zeolite structures is fundamentally affected by the Al and Si sources. Sources of Al and Si with suitable solubility and the presence of stable zeolite *BEA seeds allow kinetic control to direct the exclusive formation of *BEA zeolite up to a relatively high yield of 58%. Then, however, the MOR zeolite phase appears in the product and its formation becomes predominant. This study demonstrates the crucial importance of kinetic control for the selective formation of metastable zeolites in the OSDA-free synthesis.*

Keywords: Zeolite Beta; Hydrothermal synthesis; Mechanisms; Crystallization; OSDAs-free synthesis

1. Introduction

The synthesis of zeolites without using organic structure-directing agents (OSDA) is an environmentally friendly alternative for the production of zeolites, which avoids the use of toxic organic molecules with quaternary ammonium ions associated with the formation of wastewater containing organo-nitrogen compounds during zeolite separation and hazardous off-gases during calcination after the zeolite synthesis. However, OSDA-free synthetic procedures are available for less than 30 zeolite structures [1], and are often associated with difficulties in controlling the purity of the zeolite phase and low rates of crystallization and product yields, and are restricted to certain compositions of the zeolites [2-5]. Zeolite Beta (*BEA), which belongs to the most important zeolitic structures for catalysis, is traditionally produced using organic templates [6-8]. *BEA zeolites with Brønsted acid sites in a readily accessible 3D channel system with 12-membered rings openings are employed in industrial processes for alkylation of aromatics and isomerization of paraffins during processing of aromatics and production of automotive fuels [9, 10]. Recently, several OSDA-free procedures have been developed for the synthesis of *BEA zeolite providing zeolites with high crystallinity in a narrow range of Si/Al molar ratios from 4 to 6 [11-16]. *BEA zeolite seeds added to the synthesis gel direct the crystallization of zeolite crystals in the OSDA-free synthesis where precisely defined synthesis conditions allow the growth of crystals from the added seeds or their fragments [11-14]. Unlike syntheses involving OSDA where the agent serves as a template for the formation and stabilization of the zeolite structure during the synthesis, crystallization of the *BEA zeolite is controlled only kinetically in OSDA-free synthesis and nucleation and formation of other zeolite phases must be vastly slower than the formation of the desired structure. However, the composite building units, such as *mor*, *bea*, and *mtw* (Figure 1) of which the *BEA zeolite structure is composed, are common to other zeolite structures, and kinetic control of the growth of exclusively the *BEA zeolite is difficult. In addition, *BEA zeolite is characterized by a high molar volume of $39.4 \text{ cm}^3 \text{ mol}^{-1}$ associated with limited thermodynamic stability during synthesis without OSDA. Zeolites with high molar volume may undergo transformation to zeolites with higher density of the structural lattice, with greater stability [1]. The absence of an organic template in the synthesis gel, which otherwise stabilizes the resulting *BEA zeolite, allows the use of only conditions where the *BEA zeolite is formed in its Al-rich form with a very low Si/Al ratio of 4 – 6 [11-15] and with relatively low yield [11, 12, 15]. However, even Al-rich zeolite *BEA zeolites are regarded as promising materials for a variety of applications in catalysis in synthesis of fine chemicals and petrochemistry and in redox catalysis for selective catalytic reduction of nitrogen oxides [17-20]. Compared to

conventionally used silicon rich *BEA zeolites with Si/Al ratio ≥ 10 , these Al-rich analogues (Si/Al ratios $\sim 4 - 6$) have the potential for tailoring their catalytic properties and functionalization using much larger concentrations and variability of their active sites. Recent studies showed that both the activity and the selectivity in alkylation and hydroamination of aromatics [13, 14] and hydroisomerization and hydrocracking of paraffins [13, 21, 22] exceed that of the Si-rich H-*BEA zeolites.

The Al-rich *BEA zeolite grows from the added zeolite seeds into the amorphous phase and nucleation from the synthesis gel during the *BEA zeolite OSDA-synthesis does not occur [11, 15]. Synthesis studies under various conditions have shown that crystalline *BEA zeolite can be prepared without OSDA in relatively low yields (approx. 20 - 30%) and mordenite (MOR) zeolite is easily formed as a by-product [12, 15]. As the Al-rich *BEA zeolites are synthesised using OSDA-free syntheses that tend to be susceptible to the formation of different zeolite phases, understanding of the decisive parameters for the synthesis and controlling of competitive growth of zeolite phases is a key factor in the reliable synthesis of Al-rich *BEA zeolites.

In our work, based on an HR-TEM study complemented with XRD analysis, we describe how different zeolite phases are competitively formed during the hydrothermal synthesis and, based on a study of the effect of synthesis conditions, define the synthetic conditions for the formation of pure *BEA phase in high yields.

2. Experimental

2.1 Synthesis of zeolites

All the OSDA-free hydrothermal syntheses of Al-rich *BEA zeolites were performed with synthesis gel of molar composition 1 Si : 0.13 Al : 0.4 NaOH : 9 H₂O and typically using 5 - 20 wt% seeds of Si-rich *BEA zeolites. The synthesis gel was prepared as follows. A source of Al was added to an aqueous solution of NaOH and the mixture was stirred for 30 min at ambient temperature. After a colloidal silica sol was added and the suspension was stirred for 3 h. Si-rich *BEA zeolite as a seeding was added into the suspension and the final mixture was stirred for 30 min. The prepared synthesis gel was transferred to a stainless-steel autoclave (0.55 l, VSK Pardubice) and stirred (anchor stirrer, 30 rpm) at 120 °C or 140 °C, typically for 120 h and 50 h, respectively. The autoclave was then cooled to 90 °C and depressurized. The solid product was recovered by filtration, thoroughly washed with demineralized water and dried at 80 °C overnight. A 2.2 l stainless-steel autoclave (Büchi AG, anchor stirrer, 30 rpm) was used to study the effect of the synthesis time, where 2 ml samples were taken sequentially. The

samples were centrifuged, air dried and analysed by HR-TEM, HR-SEM and XRD methods. The combinations of the individual Al and Si sources, the temperature and the synthesis time for the individual zeolite syntheses are given in Table 2. The following Al sources were used. Amorphous Al(OH)₃ (Geloxal, IQE GROUP 83012-AH), Boehmite γ -AlO(OH) (Sasol 535100 (lot: 76674)), Gibbsite γ -Al(OH)₃ (Honeywell 239186 (lot: H0580)), NaAlO₂ (Sigma Aldrich 13404 (lot: SZB1250V) and Al(NO₃)₃·9H₂O (Sigma Aldrich 237973 (lot: BCBN7679V)). The following colloidal silicas with 40wt.% SiO₂ and different SiO₂ particle sizes were used as Si sources. Ludox (Sigma Aldrich 420808 (lot: MKBB4143)) denoted as SiO₂/8 nm, Bindzil (AkzoNobel 200N-30) denoted as SiO₂/4 nm, Kostrosol (CWK, 2040 AS) denoted as SiO₂/3 nm, and - Ludox (Chempoint (lot: 2010850304)) denoted as SiO₂/2 nm. Three Si-rich *BEA zeolites (Zeolyst CP806EL, Si/Al 10.5; Zeolysts CP814B-25, Si/Al 12.5; and Zeolysts CP814C-38, Si/Al 18) were used as the seeds. The zeolites were calcined at 500 °C or 580 °C for 4 hours before use as seeds. The type and amount of seeds used for the individual zeolite syntheses are given in Table 2. The zeolite yield was calculated using the equation

$$Y(\%) = \frac{m_{\text{obtained zeolite}}(g)}{(m_{\text{SiO}_2}(g)) + (m_{\text{Al}_2\text{O}_3}(g)) + m_{\text{*BEAseeds}}(g) + (m_{\text{Na}}(g))} * 100$$

where m_{SiO_2} , $m_{\text{Al}_2\text{O}_3}$ and m_{Na} are the amounts of SiO₂, Al₂O₃ and Na used for preparation of the synthesis gel.

2.2 Structural analysis

A High Resolution Transmission Electron Microscope (HR-TEM) JEM-2100Plus (JEOL) with accelerating voltage of 200 kV and La-B₆ filament as the electron source and a High Resolution Scanning Electron Microscope (HR-SEM) Hitachi S 4800-I were used for microscopic analysis of the products of the zeolite synthesis. The synthesis product was cast on a lacey carbon copper grid before measuring the HR-TEM images. An X-ray diffractometer MiniFlex 600 (Rigaku) with a copper anode as a source of radiation was used for X-ray diffraction (XRD) analysis. Nitrogen adsorption at liquid nitrogen temperature, measured by the 3FLEX adsorption unit (Micrometrics), was used to determine the microporous volume of the zeolites. Prior to measurement, the samples were placed in a vacuum at 400 °C for 24 h. The chemical composition of the products was determined by XRF elemental analysis using an XRF analyser (Axios). The nanoparticle size distribution in colloidal silica used as a source of Si for the synthesis of *BEA zeolites was analysed by a Malvern zeta-size analyser.

3. Results and Discussions

3.1 Effect of Al on the crystallization of *BEA structure

The effect of the Al source on the crystallization of the *BEA structure during the OSDA-free synthesis is shown in Figure 2 and Table 2. The readily-soluble Al sources of NaAlO₂ and Al(NO₃)₃ lead to the formation of a practically amorphous product or to the formation of analcim zeolite. Poorly soluble Al sources such as alumina with crystalline structures (Boehmite and Gippsite) provide the *BEA zeolite, however with very low crystallinity. Among all the Al sources tested, only the use of amorphous Al(OH)₃ yielded Al-rich *BEA zeolite with high crystallinity without admixtures of other zeolite phases. Appropriate release of aluminium ions for incorporation into the zeolite structure during the synthesis appears to be one of the driving factors for synthesis of Al-rich *BEA zeolite. A high concentration of available ions from NaAlO₂ or limitedly available Al ions from the crystalline forms of Al₂O₃ do not allow the formation of the crystalline structure of the Al-rich *BEA zeolite.

Nitrogen adsorption at liquid nitrogen temperature (Figure S1) for the zeolite obtained using amorphous Al(OH)₃ yielded a microporous volume of 0.18 cm³g⁻¹, indicating a well-developed zeolitic structure consistent with high intensity XRD lines and the absence of a signal for the amorphous phase. The ²⁷Al MAS NMR measurements (Figure S1) indicates predominant tetrahedral coordination of Al in the zeolite lattice. The synthesis using amorphous Al(OH)₃ thus yields a well-developed *BEA zeolite with high Al concentration in the zeolite lattice corresponding to a molar Si/Al ratio of 4.2. Previous studies have shown that direct incorporation of a large concentration of Al into the crystal lattice of the zeolite during the OSDA-free synthesis results in a non-defective structure of the *BEA zeolite with a predominant majority of Al in the framework [13, 22, 23] in contrast to the postsynthetic alumination of *BEA zeolite, which leads to the development of a defective structure with the presence of extra-framework Al species [24]. The highly regular organization of the structure of Al-rich *BEA zeolite prepared by OSDA synthesis was also demonstrated by Sasaki et al. [25] using detailed HR-TEM analysis of the crystalline framework of Al-rich *BEA zeolites. Compensation of the negative charge of the zeolite lattice exclusively with sodium ions during the OSDA-free synthesis allows a higher density of Al atoms in the framework compared to OSDA-assisted synthesis, where the available space in the environment of zeolite channels limits the number of bulky OSDA molecules. The detailed description of regular tetrahedral coordination of Al atoms in the framework of Al-rich *BEA zeolites prepared by OSDA-free synthesis and the population of individual AlSiAl sequences in the framework was reported in our earlier study [23].

3.2 Effect of Si on the crystallization of *BEA structure

Previous studies have used colloidal or fumed silica or freeze-dried silica powder as the Si source for the OSDA-free synthesis of Al-rich *BEA zeolite [11-16]. In our work, we focused on study of the synthesis using colloidal silica solutions, which are preferred for the production of zeolites. Figure 2 shows the effect of the particle size of colloidal silica as a Si source on the crystallization of *BEA and the formation of undesired zeolite structures in the OSDA-free synthesis of Al-rich *BEA zeolite. Note that all the other synthesis parameters, including identical Al/Si/Na/H₂O/seed ratios, were kept constant for all the syntheses. The X-ray powder diffractograms of the synthesis products showed that the size distribution of SiO₂ nanoparticles in colloidal silica affects both the intensity of the diffraction lines characteristic of the *BEA zeolite as well co-formation of other zeolite phases. Very small silica nanoparticles (2 – 3 nm) as the source of Si provide slightly less crystallinity and lead to the formation of a small amount of mordenite. Silica with particles of about 4 nm led to higher *BEA crystallinity and mordenite formation was not observed. The use of colloidal silica with larger SiO₂ particles then resulted in a product with lower crystallinity. The crystallization of *BEA zeolite is clearly influenced by the Si source, but to a much lesser extent than by the Al source. Although not very common in the synthesis of zeolites, for some hydrothermal syntheses it has been shown that the reaction of silica and the formation of a precursor for the product formation itself is a rate determining step in the synthesis [1, 4]. The results for synthesis of Al-rich *BEA zeolite indicate that the release of Si from its source and/or the formation of a precursor species influences the crystalline structure of the *BEA zeolite and that optimal size of the SiO₂ nanoparticles in the Si source can improve the product crystallinity.

3.3 Effect of seeds on the crystallization of *BEA structure

There is a consensus in the literature that Al-rich *BEA zeolite cannot crystallize during OSDA-free hydrothermal synthesis without the presence of zeolite seeds added to the synthesis gel so that the seeds provide a growth surface for crystallization of new *BEA crystals [11, 12, 15]. *BEA zeolite seeds can be considered as a type of SDA during OSDA-free hydrothermal synthesis [5] and the different composition and structures of the seeds can have a major effect on the crystallization of the zeolite [26]. For OSDA-assisted synthesis of *BEA zeolite, Bok et al. [26] showed that the molar Si/Al ratio of the seeds changes the mechanism of seeding from “core–shell” to a “dissolution” mechanism, where *BEA zeolite seeds with an Si/Al ratio of 12 do not dissolve under the conditions of hydrothermal synthesis and crystal growth on their surface results in the formation of large polycrystals, whereas seeds with a high Si/Al ratio are

partly dissolved to form small fragments, which serve as individual nuclei for the formation of nanocrystallites [26]. The effect of the Si/Al ratio and seed pre-treatment on the crystallinity of *BEA zeolite for the OSDA-free synthesis is shown in Figure 3 and Table 2. When zeolite seeds with a high Si/Al ratio of 18 were used, practically no crystalline *BEA zeolite was observed and only a broad signal indicating the presence of an amorphous phase is present in the diffractogram (Figure 3). Zeolite seeds with Si/Al equal to 12.5 provided a significantly more crystalline product while a decrease in Si/Al in the seeds to 10.5 further significantly improved the crystallization and the phase purity of the *BEA zeolite. In contrast to OSDA-assisted synthesis, only seeds with a composition and the structure that does not allow their rapid dissolution under hydrothermal synthesis conditions [16, 27] enable the formation of crystalline products in the OSDA-free synthesis.

A comparison of the crystallinity of the products obtained using zeolite seeds calcined at 500 °C and 580 °C (Figure 3 and Table 2) shows that significantly greater crystallinity can be achieved using seeds calcined at higher temperatures. Earlier studies showed that calcination of Al-rich *BEA zeolites at 580 °C leads to the abundant formation of Al-Lewis centres and corresponding local defects in the crystal structure [28]. It is also known that, when calcining an OSDA-containing zeolite at a temperature of 500 °C, a small amount of the carbonaceous deposits formed during the decomposition of OSDA remains on the surface defects of the zeolite crystal and a higher temperature is required to remove them [29]. We can speculate that the formation/release of an appropriate amount of local defects on the zeolite seeds allows for more efficient crystallization, which would explain the significantly higher crystallinity obtained using seeds calcined at 580 °C. Note that a higher calcination temperature (above 600 °C) had an adverse effect on the crystallinity of the product. It can be summarised that the Si/Al molar ratio of the zeolite seeds and their structure significantly affect the crystallization, while low Si/Al ratios, providing sufficient stability in the alkaline environment of the synthesis gel and adequate seed defectivity, have a positive effect on the crystallization of Al-rich *BEA zeolite.

3.4 *BEA zeolite as a metastable phase

The evolution of the crystalline phases during optimised OSDA-free synthesis of Al-rich *BEA zeolite analysed by XRD as a function of the synthesis time at 120 and 140 °C is shown in Figure 4. For a synthesis temperature of 120 °C, the induction period for the formation of an XRD-detectable *BEA crystalline phase is about 40 hours; then the crystallinity increases and a maximum is reached after 120 hours, whereas longer synthesis times lead to a dramatic

decrease in the crystallinity in the *BEA structure and the formation of the MOR structure. An increase in the synthesis temperature to 140 °C resulted in halving the induction period and the time to obtain BEA zeolite maximum crystallinity was reduced to 50 hours. The narrow interval of synthesis time where a highly crystalline product with respect to the *BEA structure is obtained and the subsequent rapid development of the MOR zeolite associated with the decrease in *BEA crystallinity clearly indicates that the *BEA zeolite formation is controlled kinetically. In addition to optimizing the composition of synthesis gel and temperature, strict control of synthesis duration is an essential parameter for obtaining high crystallinity of the Al-rich *BEA zeolite without mordenite formation during the kinetically controlled synthesis.

The evolution of the structure of the zeolites, the transformation of the amorphous phase and the zeolites themselves were analysed using a combination of HR-SEM and HR-TEM techniques (Figure 5). In the induction period of the synthesis, the microscopy micrographs show an amorphous phase (Figure 5A and 5B) with the presence of added seed crystals (Figure 5C). The seeds of the Si-rich zeolite are composed of nanocrystals with a size of 10 - 20 nm agglomerated into solid aggregates before their addition to the synthesis gel (Figure S2). Under hydrothermal synthesis conditions, these aggregates disintegrate to form nanocrystals dispersed in the synthesis gel (Figure 5C).

Small but well-developed zeolite crystals of a uniform morphology of partially truncated octahedrons characteristic of Al-rich *BEA zeolites [28, 30] are formed in the amorphous synthesis gel after the induction period the synthesis (Figure 5D-F). The amount of amorphous phase decreases until it completely disappears and the zeolite *BEA crystals grow until they reach a size of 0.2 - 0.5 μm , while retaining their characteristic development of morphology with the synthesis time (Figures 5G-J). This indicates a different crystallization mechanism compared to OSDA-assisted synthesis of *BEA zeolites, where initially particles having poor long-range order and an oblate morphology are formed in the synthesis gel and later transformed into zeolite crystals with longer-range order and a crystalline morphology during the synthesis [31]. Based on HR-TEM analysis of the atomic-level structure of the zeolite and visualization of the A and B polytype subdomains in the *BEA zeolite, Sasaki et al. [25] proposed that the crystals are formed by gradual deposition of a new *BEA layer on a (001) surface at the tip of a crystal in OSDA-free synthesis. Such a mechanism of crystallization is consistent with our observation of the gradual growth of well-defined crystals during synthesis. The mechanism of crystallization is characteristic of the formation of the low-defect structure of Al-rich *BEA zeolites with typically fewer defects than for OSDA-assisted synthesis [25]. Figures 5K and 5L show characteristic micrographs of the products at long synthesis times,

where XRD analysis confirmed the presence of MOR zeolite and already low zeolite *BEA crystallinity. The micrographs show the presence of MOR zeolite crystals with a characteristic morphology, which is different from the morphology of the *BEA zeolite, and formation of deformed zeolite *BEA crystals (Figure 5L). Figures 5M-O show characteristic micrographs of products at very long synthesis times with the exclusive presence of MOR zeolite crystals without *BEA zeolite crystals (at 90 h and 200 h for syntheses at 140 °C and 120 °C, respectively). A detailed analysis of the morphology of the zeolite *BEA crystals during the transition phase time is shown in Figure 6. The sharply cut edges and the smooth surface of the *BEA zeolite crystal become rounded and roughened as the synthesis time is extended to 145 hours at 120 °C, and the crystals get smaller. At the same time, well-developed MOR crystals of zeolite appear in the products. It is evident from the observations that the already formed and well-developed *BEA zeolite crystals are gradually dissolved as the synthesis time increases, and zeolite crystals of the MOR structure are formed from the dissolved material. This indicates that the synthesis is a dynamic, kinetically controlled process, where crystallization and dissolution take place and the conditions of the synthesis control the formation of the individual structures. The stability of individual zeolitic structures is associated mainly with their enthalpy and the molar volume of the zeolite, where zeolites with higher framework densities tend to be more thermodynamically stable [1, 3]. The smaller molar volume for zeolite MOR compared to *BEA, 35.4 and 39.4 cm³.mol, respectively [3], and the common building unit *mor* for both structures can contribute to the transformation of the *BEA to the MOR structure. We did not observe any structures indicating that the *BEA structure can be gradually recrystallized directly to form the MOR zeolite, and the mechanism is thus associated with the crystallization and dissolution of the already formed *BEA crystals and the subsequent formation of the MOR zeolite from the dissolved Si and Al material. Under optimised synthesis conditions with respect to the source of Al and Si and the structure of the seeds, *BEA zeolite crystals are first exclusively formed up to a yield of 58% and their dissolution and recrystallization to the MOR zeolite occur only at excessively long synthesis times. Competitive crystallization of *BEA and MOR zeolites is absent under the optimized synthesis conditions due to kinetically preferred growth of the *BEA structure on the zeolite seeds; however, because of the lower thermodynamic stability of the *BEA structure compared to the MOR zeolite after completion of crystallization of the *BEA zeolite, competitive parasitic growth of the MOR zeolite occurs at the expense of the *BEA crystals, which gradually dissolve completely due to the nonequilibrium dynamic crystallization/dissolution process. The crystallization of the *BEA zeolite and its transformation to MOR is an example of Ostwald's rule of stages [32], where

crystallization from solutions begins with the formation of thermodynamically metastable phases, followed by recrystallization to more thermodynamically stable phases. The importance of the kinetic control of *BEA crystallization and its ready gradual recrystallization to MOR zeolites can be explained by very small differences in the enthalpies of formation of these zeolite structures from the oxides ($\Delta H_{\text{ox}:298:15 \text{ K}}$) [1], where $\Delta H_{\text{ox}:298:15 \text{ K}}$ was reported to be $-2.4 \pm 2.8 \text{ kJmol}^{-1}$ and $-6.5 \pm 0.4 \text{ kJmol}^{-1}$ for *BEA and MOR, respectively [33]. In general, the dissolution of zeolites under hydrothermal conditions is controlled by the degree of undersaturation of the synthesis gel associated with chemical driving forces given by the concentration of the Al and Si source as well as the concentrations of the mineralization agent and water and the temperature [2]. The dissolution of *BEA is apparently given by the undersaturation of the synthesis gel, which arises from the gradual depletion of Al- and Si-containing species from the synthesis gel by the crystallization of MOR.

Analysis of the evolution of the individual crystalline phases under OSDA-free synthesis conditions showed that Al-rich *BEA zeolite forms a metastable phase that undergoes recrystallization changes over the synthesis time via dissolution of *BEA zeolite crystals and nucleation and growth of new mordenite crystals. The synthesis is a dynamic, kinetically controlled process where only slightly prolonged synthesis enables competitive growth of more stable MOR phases resulting in a drastic decrease in the *BEA zeolite crystallinity and formation of large amounts of mordenite.

Conclusions

The structural transformations during crystal formation and competitive growth of the zeolite phases were systematically analysed in the hydrothermal OSDA-free synthesis of Al-rich *BEA using seeding of calcined Si-rich *BEA zeolite. The effects of the source of Al and Si used for the preparation of aluminosilicate synthesis gel, temperature and duration of the synthesis, and the structure of the zeolite seeds were explored in order to identify the conditions for the crystallization of the *BEA zeolite and their influences on the zeolite phase transitions.

The study showed that *BEA zeolite is formed according to Ostwald's rule of stages as a metastable phase and completion of its crystallization is immediately followed by gradual dissolution of the *BEA crystals and more thermodynamically stable MOR zeolite crystallizes from the released Si and Al. The kinetically controlled crystallization of the *BEA zeolite is significantly affected by the structure of the seeds used and optimal crystallization takes place on seeds with a low molar ratio (Si/Al ~ 10) with a certain number of defects but with a well-preserved crystalline structure. The selective crystallization of the *BEA zeolite without the

formation of other zeolite phases is conditioned by the gradual release of Al and Si from their sources, whereas a sparingly soluble or a very well-soluble source forms conditions kinetically advantageous for the formation of other zeolite phases and MOR and ANA zeolites are produced under otherwise identical conditions. A combination of precise optimization of the synthesis time and Al and Si sources to enable the formation of a metastable *BEA zeolite phase with high yields is thus crucial for the synthesis of highly-crystalline and pure zeolite phases.

Acknowledgements

Financial support from the Czech Science Foundation under Project No. 18-20303S is greatly appreciated. The authors acknowledge the assistance provided by the Research Infrastructure NanoEnviCz under Projects No. LM2018124 and No. CZ.02.1.01/0.0/0.0/16_013/0001821 supported by the MEYS of the Czech Republic.

References

- [1] M.D. Oleksiak, J.D. Rimer, Synthesis of zeolites in the absence of organic structure-directing agents: factors governing crystal selection and polymorphism, *Reviews in Chemical Engineering*, 30 (2014) 1-49.
- [2] C.S. Cundy, P.A. Cox, The hydrothermal synthesis of zeolites: Precursors, intermediates and reaction mechanism, *Microporous and Mesoporous Materials*, 82 (2005) 1-78.
- [3] A. Navrotsky, O. Trofymuk, A.A. Levchenko, Thermochemistry of Microporous and Mesoporous Materials, *Chemical Reviews*, 109 (2009) 3885-3902.
- [4] K. Iyoki, K. Itabashi, T. Okubo, Progress in seed-assisted synthesis of zeolites without using organic structure-directing agents, *Microporous and Mesoporous Materials*, 189 (2014) 22-30.
- [5] Y. Ji, Y. Wang, B. Xie, F.S. Xiao, Zeolite Seeds: Third Type of Structure Directing Agents in the Synthesis of Zeolites, *Comments on Inorganic Chemistry*, 36 (2016) 1-16.
- [6] M.A. Cambor, A. Mifsud, J. Perezpariente, INFLUENCE OF THE SYNTHESIS CONDITIONS ON THE CRYSTALLIZATION OF ZEOLITE BETA, *Zeolites*, 11 (1991) 792-797.
- [7] L.J. Leu, L.Y. Hou, B.C. Kang, C.P. Li, S.T. Wu, J.C. Wu, SYNTHESIS OF ZEOLITE-BETA AND CATALYTIC ISOMERIZATION OF NORMAL-HEXANE OVER PT/H-BETA CATALYSTS, *Applied Catalysis*, 69 (1991) 49-63.
- [8] J. Perezpariente, J.A. Martens, P.A. Jacobs, FACTORS AFFECTING THE SYNTHESIS EFFICIENCY OF ZEOLITE-BETA FROM ALUMINOSILICATE GELS CONTAINING ALKALI AND TETRAETHYLAMMONIUM IONS, *Zeolites*, 8 (1988) 46-53.

- [9] A. Corma, M.J. Díaz-Cabañas, J. Martínez-Triguero, F. Rey, J. Rius, A large-cavity zeolite with wide pore windows and potential as an oil refining catalyst, *Nature*, 418 (2002) 514-517.
- [10] W. Vermeiren, J.P. Gilson, Impact of zeolites on the petroleum and petrochemical industry, *Topics in Catalysis*, 52 (2009) 1131-1161.
- [11] B. Xie, J. Song, L. Ren, Y. Ji, J. Li, F.-S. Xiao, Organotemplate-Free and Fast Route for Synthesizing Beta Zeolite, *Chemistry of Materials*, 20 (2008) 4533-4535.
- [12] G. Majano, L. Delmotte, V. Valtchev, S. Mintova, Al-rich zeolite beta by seeding in the absence of organic template, *Chemistry of Materials*, 21 (2009) 4184-4191.
- [13] P. Sazama, B. Wichterlova, S. Sklenak, V.I. Parvulescu, N. Candu, G. Sadovska, J. Dedecek, P. Klein, V. Pashkova, P. Stastny, Acid and redox activity of template-free Al-rich H-BEA* and Fe-BEA* zeolites, *J. Catal.*, 318 (2014) 22-33.
- [14] B. Yilmaz, U. Muller, M. Feyen, S. Maurer, H. Zhang, X. Meng, F.S. Xiao, X. Bao, W. Zhang, H. Imai, T. Yokoi, T. Tatsumi, H. Gies, T. De Baerdemaeker, D. De Vos, A new catalyst platform: Zeolite Beta from template-free synthesis, *Catal. Sci. Technol.*, 3 (2013) 2580-2586.
- [15] Y. Kamimura, S. Tanahashi, K. Itabashi, A. Sugawara, T. Wakihara, A. Shimojima, T. Okubo, Crystallization Behavior of Zeolite Beta in OSDA-Free, Seed-Assisted Synthesis, *The Journal of Physical Chemistry C*, 115 (2011) 744-750.
- [16] Y. Kamimura, W. Chaikittisilp, K. Itabashi, A. Shimojima, T. Okubo, Critical Factors in the Seed-Assisted Synthesis of Zeolite Beta and “Green Beta” from OSDA-Free Na+–Aluminosilicate Gels, *Chemistry – An Asian Journal*, 5 (2010) 2182-2191.
- [17] P. Sazama, L. Mokrzycki, B. Wichterlova, A. Vondrova, R. Pilar, J. Dedecek, S. Sklenak, E. Tabor, Unprecedented propane-SCR-NO_x activity over template-free synthesized Al-rich Co-BEA* zeolite, *Journal of Catalysis*, 332 (2015) 201-211.
- [18] P. Sazama, J. Moravkova, S. Sklenak, A. Vondrova, E. Tabor, G. Sadovska, R. Pilar, Effect of the Nuclearity and Coordination of Cu and Fe Sites in β Zeolites on the Oxidation of Hydrocarbons, *ACS Catalysis*, 10 (2020) 3984-4002.
- [19] P. Sazama, R. Pilar, L. Mokrzycki, A. Vondrova, D. Kaucky, J. Plsek, S. Sklenak, P. Stastny, P. Klein, Remarkably enhanced density and specific activity of active sites in Al-rich Cu-, Fe- and Co-beta zeolites for selective catalytic reduction of NO_x, *Applied Catalysis B: Environmental*, 189 (2016) 65-74.
- [20] E. Tronconi, I. Nova, J. Nováková, M. Bernauer, P. Sazama, Z. Sobalík, Mechanistic Study of the NO + NH₄NO₃ Reaction on H- and Fe/H-BEA Zeolites Using ¹⁵N and ¹⁸O Labeled Species, *Topics in Catalysis*, 61 (2018) 1967-1973.

- [21] B. Xie, H. Zhang, C. Yang, S. Liu, L. Ren, L. Zhang, X. Meng, B. Yilmaz, U. Muller, F.-S. Xiao, Seed-directed synthesis of zeolites with enhanced performance in the absence of organic templates, *Chem. Commun. (Cambridge, U. K.)*, 47 (2011) 3945-3947.
- [22] T. De Baerdemaeker, B. Yilmaz, U. Muller, M. Feyen, F.S. Xiao, W. Zhang, T. Tatsumi, H. Gies, X. Bao, D. De Vos, Catalytic applications of OSDA-free Beta zeolite, *J. Catal.*, 308 (2013) 73-81.
- [23] P. Sazama, E. Tabor, P. Klein, B. Wichterlova, S. Sklenak, L. Mokrzycki, V. Pashkova, M. Ogura, J. Dedecek, Al-rich beta zeolites. Distribution of Al atoms in the framework and related protonic and metal-ion species, *Journal of Catalysis*, 333 (2016) 102-114.
- [24] K. Shanjiao, D. Tao, L. Qiang, D. Aijun, Z. Yanying, P. Huifang, Preparation and application of zeolite beta with super-low SiO₂/Al₂O₃ ratio, *Journal of Porous Materials*, 15 (2008) 159-162.
- [25] Y. Sasaki, Y. Yoshida, C.A.J. Fisher, T. Ikeda, K. Itabashi, T. Okubo, Polytype distributions in low-defect zeolite beta crystals synthesized without an organic structure-directing agent, *Microporous and Mesoporous Materials*, 225 (2016) 210-215.
- [26] T.O. Bok, E.P. Andriako, E.E. Knyazeva, I.I. Ivanova, Engineering of zeolite BEA crystal size and morphology: Via seed-directed steam assisted conversion, *RSC Advances*, 10 (2020) 38505-38514.
- [27] J. Devos, M.A. Shah, M. Dusselier, On the key role of aluminium and other heteroatoms during interzeolite conversion synthesis, *RSC Advances*, 11 (2021) 26188-26210.
- [28] S.F. Rastegar, G. Sadvoska, R. Pilar, J. Moravkova, D. Kaucky, L. Brabec, J. Pastvova, P. Sazama, Analysis of decisive structural parameters of zeolites for alkylation of benzene with ethylene, *Applied Catalysis A: General*, 591 (2020).
- [29] I. Jirka, P. Sazama, A. Zikánová, P. Hrabánek, M. Kocirik, Low-temperature thermal removal of template from high silica ZSM-5. Catalytic effect of zeolitic framework, *Microporous and Mesoporous Materials*, 137 (2011) 8-17.
- [30] P. Sazama, D. Kaucky, J. Moravkova, R. Pilar, P. Klein, J. Pastvova, E. Tabor, S. Sklenak, I. Jakubec, L. Mokrzycki, Superior activity of non-interacting close acidic protons in Al-rich Pt/H-*BEA zeolite in isomerization of n-hexane, *Applied Catalysis A: General*, 533 (2017) 28-37.
- [31] N.D. Hould, R.F. Lobo, Nanoparticle Precursors and Phase Selectivity in Hydrothermal Synthesis of Zeolite β , *Chemistry of Materials*, 20 (2008) 5807-5815.
- [32] J. Nývlt, The Ostwald Rule of Stages, *Crystal Research and Technology*, 30 (1995) 443-449.

[33] R. Mathieu, P. Vieillard, A predictive model for the enthalpies of formation of zeolites, *Microporous and Mesoporous Materials*, 132 (2010) 335-351.

Table 1. Structural information of *BEA and MOR zeolite framework types.

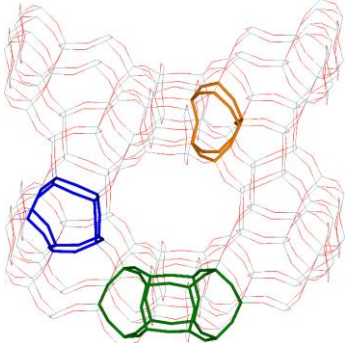
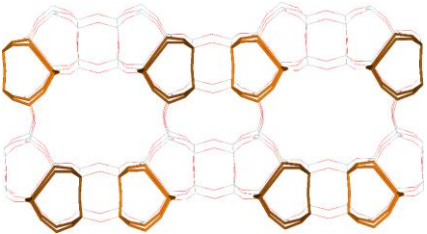

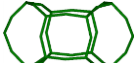
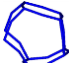

	*BEA	MOR
<i>Structure illustration</i>		
<i>Composite building units</i>	   <i>mor (t-tes)</i> <i>bea</i> <i>mtw (t-mtw)</i>	 <i>mor (t-tes)</i>
<i>Molar volume</i>	39.4 cm ³ mol ⁻¹	35.4 cm ³ mol ⁻¹
<i>Rings</i>	12, 6, 5, 4	12, 8, 5, 4
<i>Pores</i>	3D	1D

Table 2. Parameters of the OSDA-free hydrothermal syntheses of Al-rich *BEA zeolites.

Product	Sources of Al ^a and Si ^b	*BEA seeds	Time / Temperature	Crystallinity ^c	Si/Al ^d	Yield
		T _{calc} / Si/Al /Amount		(%)		(%)
<i>Effect of Al source</i>						
*BEA	Al(OH) ₃ /SiO ₂ 4 nm	580°C/10.5/10%	50 h/140°C	100	4.2	58
*BEA+MOR	Boehmite/SiO ₂ 4 nm	580°C/10.5/10%	50 h/140°C	58	4.8	-
MOR	Gibbsite/SiO ₂ 4 nm	580°C/10.5/10%	44 h/140°C	6	-	-
P zeolite	NaAlO ₂ /SiO ₂ 4 nm	580°C/10.5/10%	40 h/140°C	0	-	-
ANA	Al(NO ₃) ₃ /SiO ₂ 4 nm	580°C/10.5/10%	48 h/140°C	0	-	-
<i>Effect of Silica source</i>						
*BEA+MOR	Al(OH) ₃ /SiO ₂ 2 nm	580°C/10.5/10%	50 h/140°C	63	-	-
*BEA+MOR	Al(OH) ₃ /SiO ₂ 3 nm	580°C/10.5/10%	50 h/140°C	73	-	-
*BEA	Al(OH) ₃ /SiO ₂ 4 nm	580°C/10.5/10%	50 h/140°C	98	4.4	57
*BEA+MOR	Al(OH) ₃ /SiO ₂ 8 nm	580°C/10.5/10%	50 h/140°C	74	5.0	-
<i>Effect of seeding</i>						
*BEA	Al(OH) ₃ /SiO ₂ 4 nm	580°C/10.5/10%	50 h/140°C	100	4.2	58
*BEA+MOR	Al(OH) ₃ /SiO ₂ 4 nm	500°C/10.5/10%	50 h/140°C	68	4.7	-
MOR+*BEA	Al(OH) ₃ /SiO ₂ 4 nm	580°C/12.5/10%	50 h/140°C	39	-	-
MOR	Al(OH) ₃ /SiO ₂ 4 nm	500°C/12.5/10%	50 h/140°C	16	-	-
“Amorphous”	Al(OH) ₃ /SiO ₂ 4 nm	580°C/18.5/10%	50 h/140°C	0	-	-
“Amorphous”	Al(OH) ₃ /SiO ₂ 4 nm	500°C/18.5/10%	50 h/140°C	0	-	-
<i>Effect of amount seeding</i>						
*BEA	Al(OH) ₃ /SiO ₂ 4 nm	580°C/10.5/10%	120 h/120°C	100	4.2	56

*BEA	Al(OH) ₃ /SiO ₂ 4 nm	580°C/10.5/5%	120 h/120°C	98	4.4	37
*BEA	Al(OH) ₃ /SiO ₂ 4 nm	580°C/10.5/15%	120 h/120°C	99	4.3	59

^a Al sources: Al(OH)₃ – Amorphous, Boehmite – Semi crystalline γ -AlO(OH), Gibbsite – crystalline γ -Al(OH)₃

^b Si sources: Colloidal silicas with 40wt.% SiO₂ with specified SiO₂ particle sizes

^c Zeolite crystallinity is calculated from XRD intensity of the most intense reflection peaks at 7.6° and 22.2° 2 Theta.

^d Molar Si/Al ratio of zeolites obtained by chemical analysis

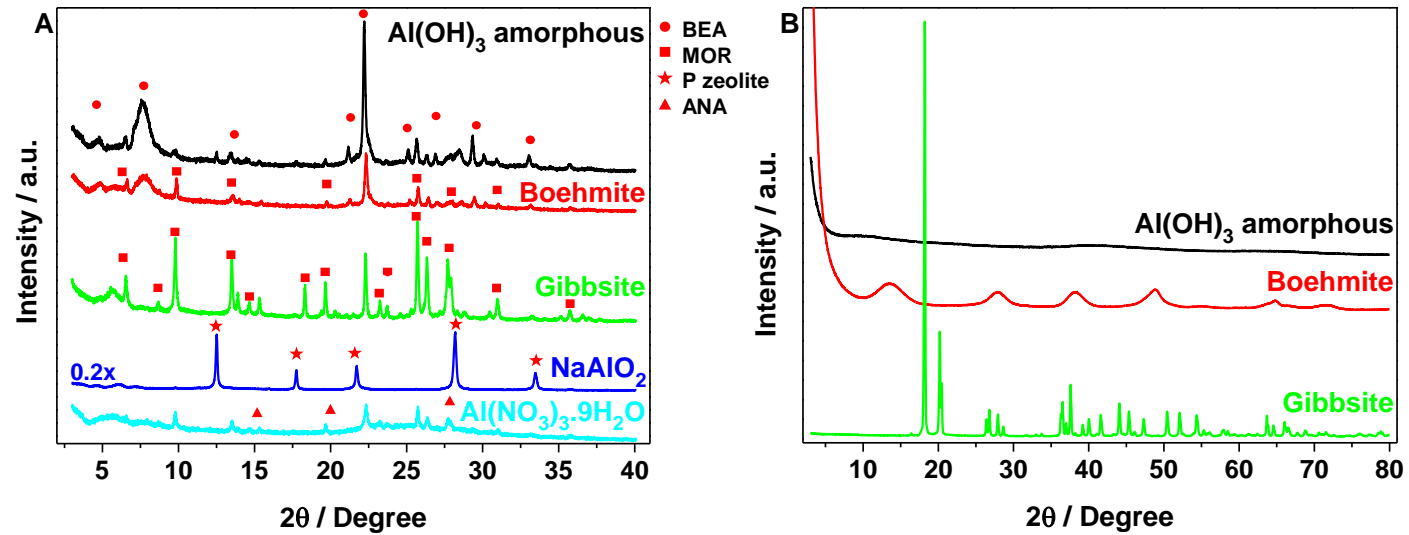


Figure 1. The effect of the Al source on the OSDA-free synthesis of Al-rich *BEA zeolite. X-ray powder diffractograms of A) synthesis products obtained using different Al sources and B) Al sources: amorphous Al(OH)_3 , Boehmite (semi crystalline) and Gibbsite (crystalline). *The crystallinity of the product was monitored during the synthesis and the diffractograms of the products are given for the synthesis times with the best results with respect to the development and purity of the *BEA zeolite (50, 50, 44, 40, and 48 h for amorphous Al(OH)_3 , Boehmite, Gibbsite, NaAlO_2 and $\text{Al(NO}_3)_3$, respectively).*

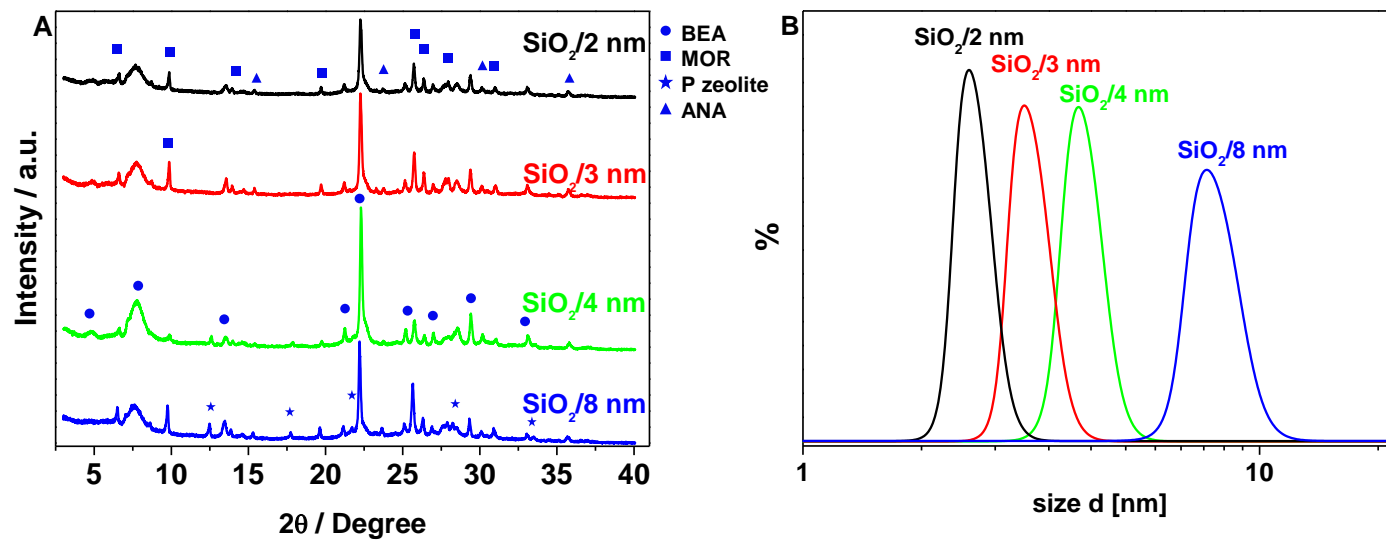


Figure 2. The effect of the particle size of the colloidal silica as a Si source on the crystallization of *BEA and the formation of undesired zeolite structures in the OSDA-free synthesis of Al-rich *BEA zeolite. A) X-ray powder diffractograms of the synthesis products and B) the size distribution of SiO₂ nanoparticles in colloidal silica analysed by zeta-size analyser.

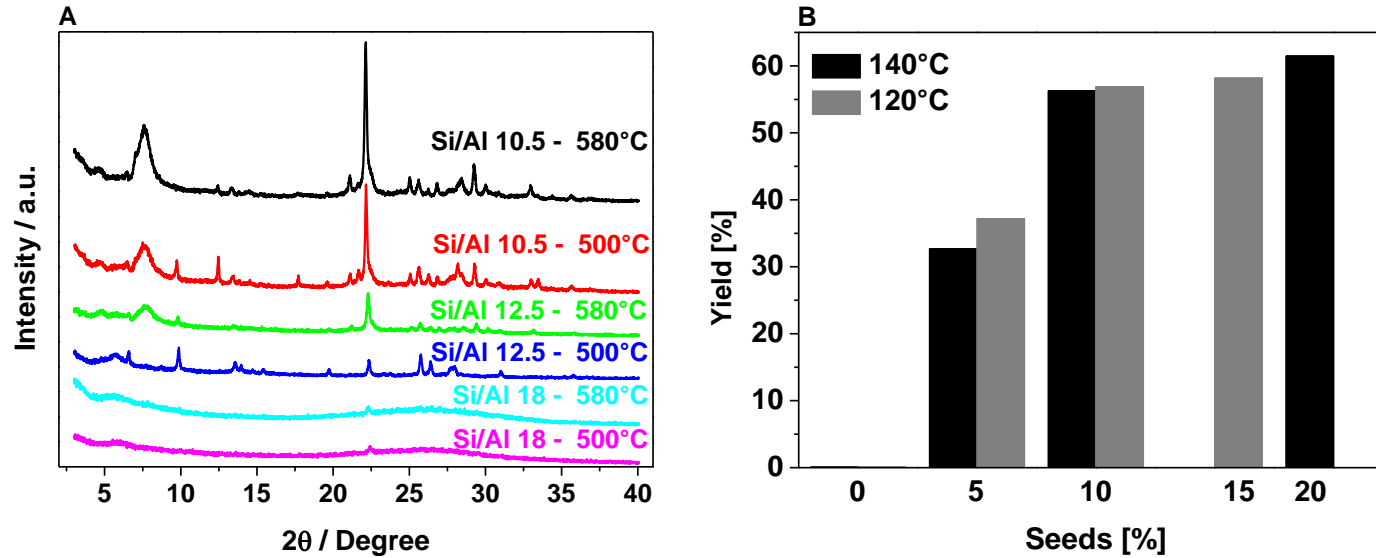


Figure 3. The effect of seeding on the OSDA-free synthesis of Al-rich *BEA zeolite. A) X-ray powder diffractograms of the synthesis products obtained using seeds with different Si/Al ratios and calcined at 500 °C and 580 °C, and B) yield of Al-rich *BEA zeolite obtained with different amounts of *BEA seeds (Si/Al 10.5 – 580°C).

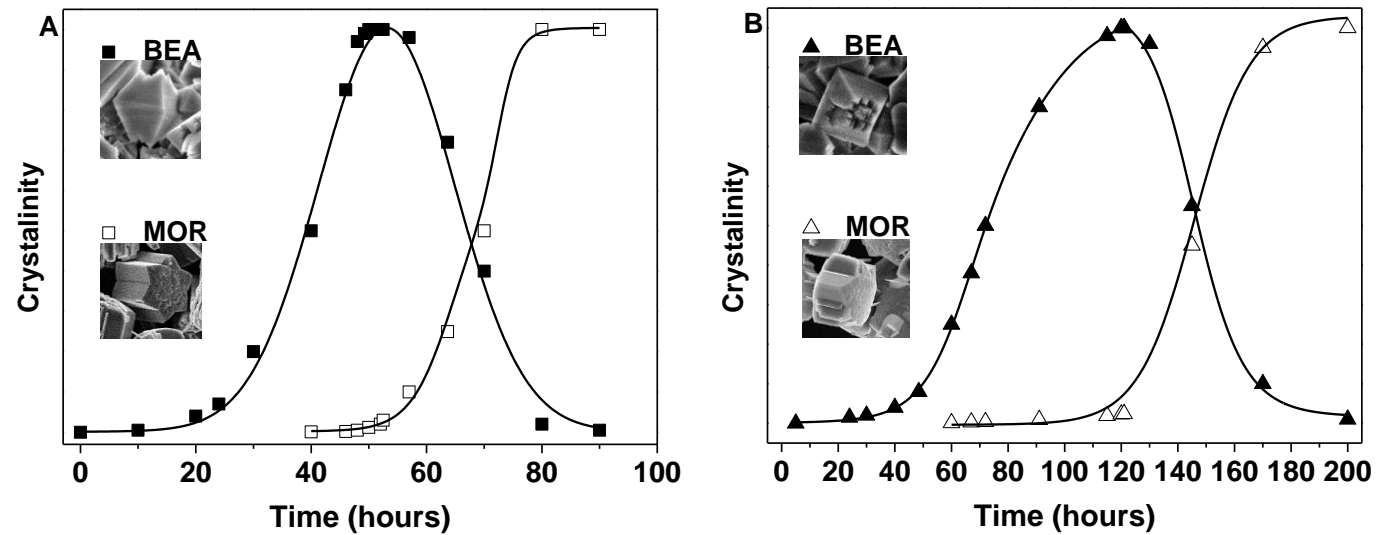


Figure 4. XRD analysis of the development of structure of *BEA and MOR zeolites as a function of the synthesis time under optimized synthesis conditions for Al-rich *BEA synthesis for temperatures A) 140 °C and B) 120 °C. *Synthesis conditions: 140 °C and 120 °C, 1 SiO₂ : 0.13 Al : 0.4 NaOH : 9 H₂O, 10 wt% seeds, amorphous Al(OH)₃ and SiO₂/4 nm as a Si and Al source, respectively.*

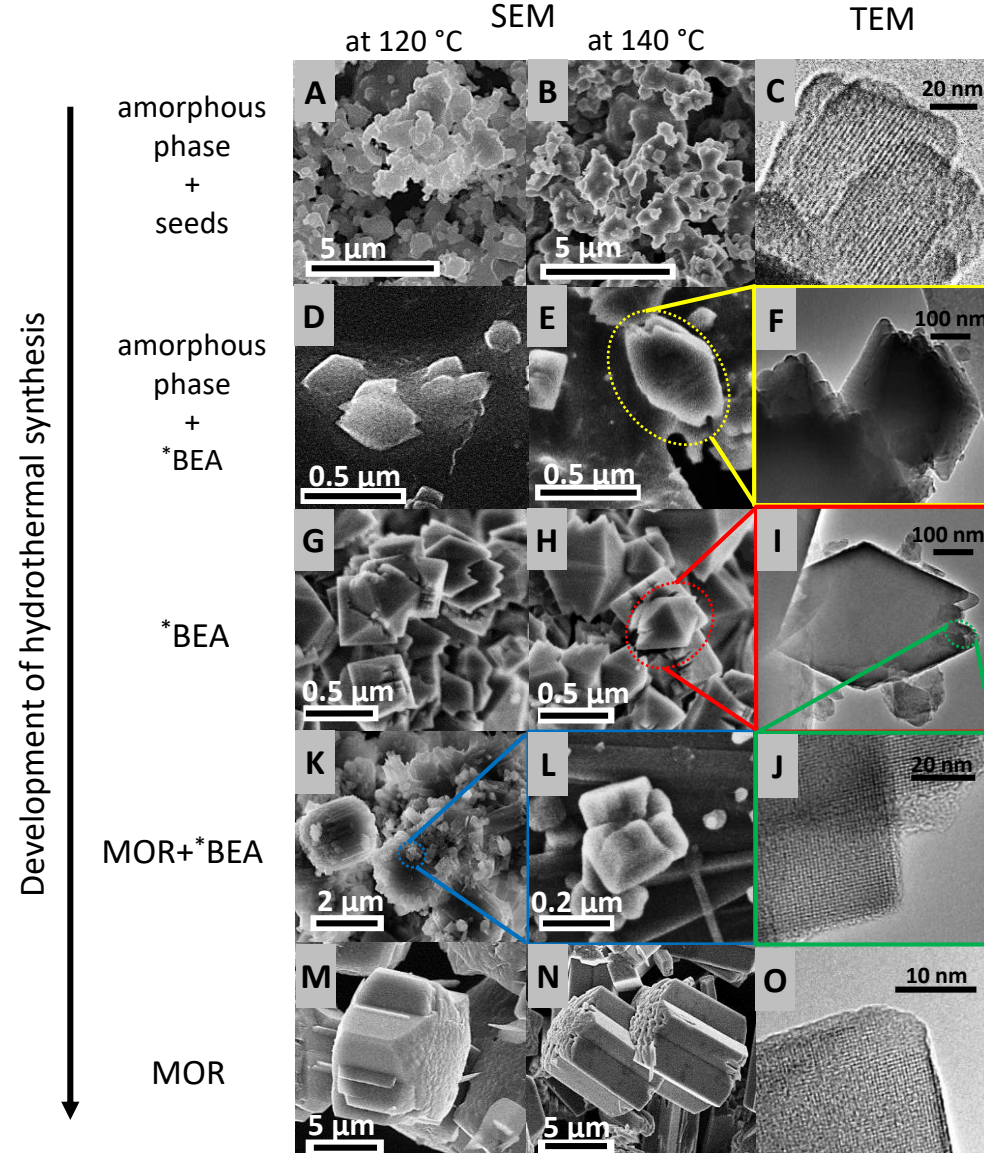


Figure 5. HR-SEM and HR-TEM analysis of the evolution of the structure of the *BEA zeolite and its transformation to the MOR zeolite during OSDA-free synthesis of Al-rich *BEA zeolite. A) and B) amorphous phase and C) seed crystals in the induction period of the synthesis. D-F) small but well-developed zeolite crystals of a uniform morphology of partially truncated octahedrons characteristic of Al-rich *BEA formed in the amorphous synthesis gel after the induction period of the synthesis. G) – J) *BEA crystals with their characteristic morphology in the fully crystalline product for an optimal synthesis duration. K) and L), MOR zeolite crystals with a characteristic morphology, which is different from the morphology of *BEA zeolite, and deformed zeolite *BEA crystals with an oblate morphology at long synthesis times. M) and O) the exclusive presence of MOR zeolite crystals without *BEA zeolite crystals at very long crystallization times.

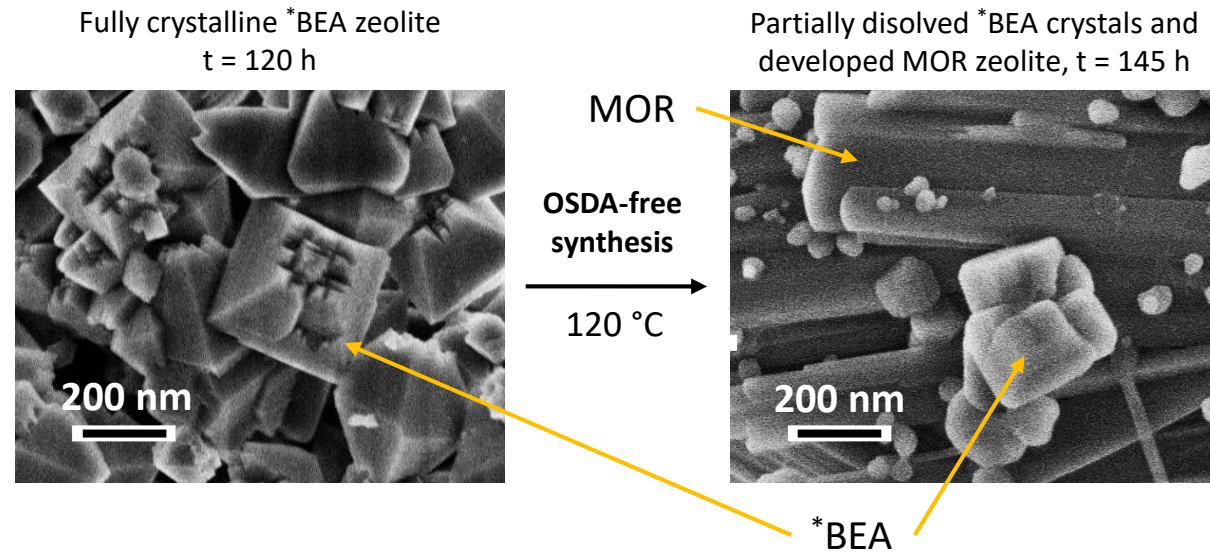


Figure 6. HR-SEM images of products of Al-rich *BEA synthesis after 120 and 145 h at 120 °C showing the transformation of zeolite *BEA by gradual dissolution of their crystals and crystallization of MOR zeolite.